14 May 2020

Thermal Transport Across the Interface between Liquid N-Dodecane and its Own Vapor: A Molecular Dynamics Study

Eric Bird

Jesus Gutierrez Plascencia

Zhi Liang
Missouri University of Science and Technology, zlch5@mst.edu

Recommended Citation

E. Bird et al., "Thermal Transport Across the Interface between Liquid N-Dodecane and its Own Vapor: A Molecular Dynamics Study," *Journal of Chemical Physics*, vol. 152, no. 18, article no. 184701, American Institute of Physics, May 2020.
The definitive version is available at https://doi.org/10.1063/1.5144279

The Journal of Chemical Physics

Thermal transport across the interface between liquid *n*-dodecane and its own vapor: A molecular dynamics study

Cite as: J. Chem. Phys. **152**, 184701 (2020); https://doi.org/10.1063/1.5144279
Submitted: 30 December 2019 • Accepted: 17 April 2020 • Published Online: 08 May 2020

Eric Bird, Jesus Gutierrez Plascencia and Zhi Liang

AIP Publishing

The Journal of Chemical Physics ARTICLE scitation.org/journal/jcp

Thermal transport across the interface between liquid *n*-dodecane and its own vapor: A molecular dynamics study

Cite as: J. Chem. Phys. 152, 184701 (2020); doi: 10.1063/1.5144279
Submitted: 30 December 2019 • Accepted: 17 April 2020 •
Published Online: 8 May 2020

Eric Bird, Jesus Gutierrez Plascencia, and Zhi Liang[a)]

AFFILIATIONS

Department of Mechanical Engineering, California State University, Fresno, California 93740, USA

[a)]Author to whom correspondence should be addressed: zliang@csufresno.edu

ABSTRACT

There are two possible thermal transport mechanisms at liquid–gas interfaces, namely, evaporation/condensation (i.e., heat transfer by liquid–vapor phase change at liquid surfaces) and heat conduction (i.e., heat exchange by collisions between gas molecules and liquid surfaces). Using molecular dynamics (MD) simulations, we study thermal transport across the liquid–vapor interface of a model *n*-dodecane ($C_{12}H_{26}$) under various driving force conditions. In each MD simulation, we restrict the thermal energy to be transferred across the liquid–vapor interface by only one mechanism. In spite of the complex intramolecular interactions in *n*-dodecane molecules, our modeling results indicate that the Schrage relationships, which were shown to give accurate predictions of evaporation and condensation rates of monatomic fluids, are also valid in the prediction of evaporation and condensation rates of *n*-dodecane. In the case of heat conduction at the liquid–vapor interface of *n*-dodecane, the interfacial thermal conductance obtained from MD simulations is consistent with the prediction from the kinetic theory of gases. The fundamental understanding of thermal transport mechanisms at liquid–gas interfaces will allow us to formulate appropriate boundary conditions for continuum modeling of heating and evaporation of small fuel droplets.

I. INTRODUCTION

Heating and evaporation of small fuel droplets are processes of great importance to the efficiency of spray combustion in various gasoline and diesel engines.[1–6] It is widely accepted that an effective approach to make engines cleaner and more efficient is to reduce the size of fuel droplets.[7] When the size of fuel droplets is below a few tens of microns, the resistance to heat and mass transfer at the liquid–gas interfaces cannot be ignored. In this case, the conventional assumption of the continuous temperature profile across the interface and the saturated vapor near the interface will lead to considerable errors in the prediction of evaporation time of fuel droplets.[1–3] To accurately model heating and evaporation of micro/nanoscale fuel droplets, it is essential to introduce the appropriate temperature and density boundary conditions at the liquid–gas interface.

Understanding the phase change and temperature jump at evaporating surfaces requires the treatment from the kinetic theory of gases (KTG).[8–12] Based on the KTG, evaporation and condensation processes have been studied for over a century, and a number of relationships that correlate the evaporation/condensation rates with the temperature and density of fluid near liquid–gas interfaces were derived.[8] Among these relationships, the two most widely used ones are Hertz–Knudsen (HK) relationships[8–10] and Schrage relationships.[11,13] Both relationships contain a parameter called mass accommodation coefficient (MAC), which is defined as the fraction of vapor molecules that strike the interface and are accommodated to the liquid phase. Accurate measurement of the MAC and the fluid temperature and density near liquid–gas interfaces remains challenging in the experiment.[8] As a result, the experimental validation of HK and Schrage relationships is very difficult.

Another difficulty in the validation of HK and Schrage relationships is that there are two thermal transport mechanisms at liquid–gas interfaces. In addition to evaporation and condensation, thermal energy could also be transferred across a liquid–gas interface

through interfacial heat conduction (i.e., heat exchange by collisions between gas molecules and liquid surfaces).[12] In diesel engines, the fuel droplets are surrounded by high temperature gases, which could result in heating of the fuel droplets through heat conduction across the liquid–gas interface. Interfacial heat conduction was often overlooked in the thermal analysis of an evaporating/condensing liquid surface. Recent numerical studies[14,15] show that heat conduction can play an important role in thermal transport across liquid–gas interfaces. However, an experimental study of heat conduction across a liquid–gas interface is also challenging since it also requires a local measurement of temperature through a very thin layer near the interface with sufficient accuracy. Moreover, evaporation and heat conduction often occur simultaneously at liquid–gas interfaces. It remains challenging in experiment to quantitatively analyze the contribution from each mechanism to the thermal transport across liquid–gas interfaces.

One way to mitigate the experimental challenges is to use molecular dynamics (MD) simulations that determine positions, velocities, and forces of all atoms in a system by numerical integration of Newton's equation of motion. MD simulations have two big advantages in the study of thermal transport across liquid–gas interfaces. First, using statistical mechanics based molecular-level formulas and time averaging, MD simulations can determine all the quantities in the relationships derived from the KTG with high fidelity and with high temporal and spatial resolutions that are difficult to achieve experimentally. This allows us to test the validities of the various relationships that model the heat and mass transfer at liquid–gas interfaces. Second, one can readily restrict the thermal energy to be transferred across the liquid–gas interface by only one mechanism in MD simulations. This allows us to elucidate what roles each mechanism plays in heat transfer across liquid–gas interfaces.

In this work, we resort to MD simulations to study thermal transport across the interface between liquid *n*-dodecane ($C_{12}H_{26}$) and its own vapor. $C_{12}H_{26}$ is close to the average chemical formula for common diesel fuel.[16] Therefore, our simulation results are relevant to the heating and evaporation of diesel fuel in diesel engines. We have shown in our previous MD studies that Schrage relationships are accurate in the prediction of evaporation and condensation rates of monatomic fluids,[17,18] and the heat conduction processes at liquid–gas interfaces of monatomic fluids are well described by the relationship derived from the KTG.[15] By comparison, the fluid *n*-dodecane is much more complex as it contains chain molecules. The complex intramolecular and intermolecular interactions in *n*-dodecane will make the interfacial thermal transport process more complex. Although numerous MD simulations have been carried out to study phase equilibria and phase change at the liquid–vapor interface of *n*-dodecane,[3–6] the validity of the relationships in the prediction of heat conduction and evaporation/condensation rates at the liquid–vapor interface of *n*-dodecane or other chain molecules has not been addressed.

To address the aforementioned gap in our knowledge, the rest of this paper is organized as follows: In Sec. II, we introduce the relationships derived from the KTG for the prediction of heat conduction and evaporation/condensation rates at liquid–gas interfaces. In Sec. III, we describe the MD model and the basic properties of the model fluid. In Sec. IV, we present results of the steady-state evaporation/condensation process and test the validity of Schrage relationships in quantifying steady-state evaporation/condensation rates. In Sec. V, we show the results of the steady-state heat conduction across the liquid–vapor interface of the model fluid and discuss them in the context of the kinetic theory based analysis. Finally, Sec. VI concludes with summary and conclusions.

II. THE RELATIONSHIPS DERIVED FROM THE KTG

A. Evaporation and condensation rate

When evaporation/condensation occurs, energy is transferred by liquid–vapor phase changes at the interface. In this case, the interfacial heat flux equals Jh_{fg}, where h_{fg} is the latent heat and J is the evaporation/condensation molar flux. To predict the evaporation/condensation heat flux, the key problem is to find relationships that are able to accurately predict J under various driving force conditions.

To model evaporation and condensation processes, both HK and Schrage relationships assume that the velocity distribution (VD) of liquid and vapor molecules near a liquid–gas interface follows the Maxwell–Boltzmann (MB) velocity distribution. This leads to an expression for the molar flux at a liquid–gas interface as [11,13]

$$J = \alpha_M \sqrt{\frac{R}{2\pi M}} \left(\rho_g(T_L) \sqrt{T_L} - \Gamma(v_R) \rho_v \sqrt{T_v} \right), \tag{1}$$

where T_L and T_v are the temperature of liquid and vapor near the liquid–vapor interface, respectively, $\rho_g(T_L)$ is the saturated vapor density at T_L, ρ_v is the density of vapor adjacent to the interface, R is the universal gas constant, M is the molar mass of fluid molecules undergoing phase change, and α_M is the mass accommodation coefficient (MAC). The MAC is defined as the fraction of vapor molecules that strike the interface and are accommodated to the liquid phase.

If J in Eq. (1) is greater than 0, net evaporation occurs. If J is less than 0, net condensation occurs. When net evaporation/condensation occurs, the vapor molecules near the liquid–vapor interface would have a nonzero mean (macroscopic) velocity normal to the interface. Accordingly, Schrage assumed that the vapor molecules adjacent to the interface have a MB velocity distribution shifted by the mean velocity, $v_{v,0}$.[11,13] Based on this assumption, the effects of macroscopic vapor motion are taken into account in Eq. (1) by the function $\Gamma(v_R)$, which is given by [11,13]

$$\Gamma(v_R) = e^{-v_R^2} - v_R \sqrt{\pi} [1 - erf(v_R)], \tag{2}$$

where v_R is the ratio of the macroscopic speed of vapor, $v_{v,0}$, to the most probable thermal speed of vapor molecules,

$$v_R = \frac{v_{v,0}}{\sqrt{2RT_v/M}}. \tag{3}$$

An important indicator of the validity of Schrage relationship is whether the velocity distribution (VD) of evaporating/condensing vapor molecules follows the shifted MB distribution. The experimental determination of VD near an evaporating/condensing surface is very challenging. One of the advantages of MD simulations is that the VD can be readily determined by MD simulations. In our previous MD study of evaporation of monatomic fluids,[17] we have shown that the VD of monatomic vapor molecules near the

evaporating surface follows the shifted MB distribution. In this work, we will use MD simulations to investigate if the assumption of the shifted MB distribution is still valid for *n*-dodecane vapor molecules near evaporating and condensing interfaces and test the accuracy of Schrage relationships in the prediction of evaporation and condensation rates of *n*-dodecane.

B. Interfacial heat conduction rate

In the case of heat conduction across liquid–gas interfaces, gas molecules exchange thermal energy with liquid surfaces through collisions/interactions with the liquid surface. Such a heat transfer mechanism is similar to that at solid–gas interfaces where gas molecules impact a surface, thermalize with the surface, and are being reflected with a temperature closer to the surface temperature. In this case, the interfacial heat flux is determined by $G_K\Delta T$, where ΔT is the temperature jump at the liquid–gas interface and G_K is the thermal conductance (Kapitza conductance) at the liquid–gas interface.[12] To determine the conduction heat flux at the liquid–gas interface, the key problem is to find relationships that are able to accurately predict G_K.

The KTG predicts that the G_K at liquid–gas interfaces is determined by the frequency of collisions between gas molecules and the liquid surface and the efficiency of the thermal energy exchange during the liquid–gas collision process.[12] For incident gas molecules with an average temperature, T_{gas}, and a density, ρ_{gas}, the liquid–gas collision frequency per area, N_{gas}, is given by [12]

$$N_{gas} = \rho_{gas}\sqrt{RT_{gas}/2\pi M_{gas}}, \tag{4}$$

where M_{gas} is the molar mass of gas molecules. The heat exchange efficiency at a liquid–gas interface can be quantified by the thermal accommodation coefficient (TAC), which is defined as

$$\alpha_T = \frac{E_r - E_i}{E_s - E_i}, \tag{5}$$

where E_i, and E_r are the average energy of incident and reflected gas molecules, respectively, and E_s is the average energy a gas would carry if it equilibrates with the liquid surface upon reflection. Accordingly, the G_K due to heat conduction at the liquid–gas interface is given by [12]

$$G_K = N_{gas}\left(c_V + \tfrac{1}{2}R\right)\frac{2\alpha_T}{2-\alpha_T}, \tag{6}$$

where c_V is the constant-volume specific heat of gas near the liquid–gas interface. In our previous studies, we have shown that Eq. (6) gives good predictions of G_K at various solid–gas interfaces[19–21] and at liquid–gas interfaces of monatomic fluids.[15] *n*-dodecane molecules are much more complex than monatomic molecules. In this work, we use MD simulations to study how the internal degrees of freedom in *n*-dodecane molecules will affect the TAC and the heat conduction rate at liquid–gas interfaces.

III. MD SIMULATION OF *n*-DODECANE

A. The MD model

Using MD simulations, we study evaporation/condensation and heat conduction across a flat liquid–vapor interface of *n*-dodecane. As depicted in Fig. 1, the typical model system consists

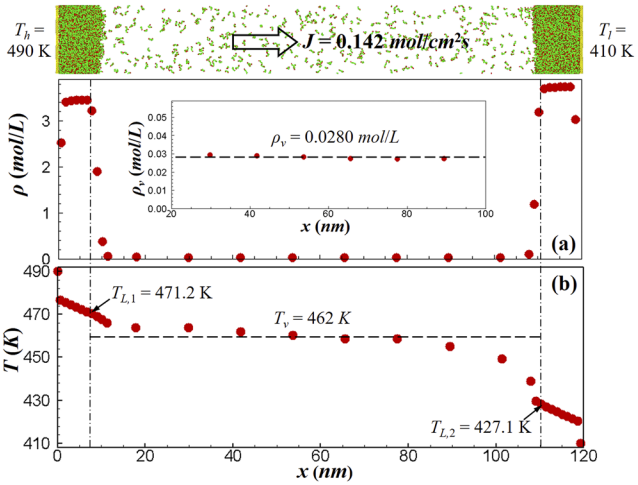

FIG. 1. (Top panel) A snapshot of the model system in the course of NEMD simulation in the representative case of T_h = 490 K and T_l = 410 K. The yellow, red, and green dots in the snapshot represent the Au atom, CH_3 pseudoatom, and CH_2 pseudoatoms, respectively. (Bottom panels) (a) Density and (b) temperature profiles at steady state in the representative case. The inset in (a) shows the density profile in the vapor region. The horizontal dashed lines indicate the average value of density and temperature in the vapor region. The vertical dashed–dotted lines indicate the location of liquid–vapor interfaces.

of fluid *n*-dodecane confined by two solid Au slabs. Each Au slab is formed by a three-layered FCC (100) plane solid Au with a cross-sectional area of 15.5 × 15.5 nm^2. On each of the two inner surfaces of the Au slabs, we place a liquid *n*-dodecane thin film. The initial thickness of the liquid layer on the left and right solid surfaces is ~10 nm and 8.5 nm, respectively. The separation between two liquid surfaces is about 101 nm. In MD simulations, periodic boundary conditions (PBCs) are applied in the y and z directions, and the atoms in the outermost Au layers are fixed. The fluid in the region from x = 12 nm to x = 108 nm is always in the gaseous state in MD simulations. Therefore, we define this region as the central vapor region of the model system.

To model the intra- and intermolecular interactions of *n*-dodecane molecules, we use the united atom (UA) model proposed by Nath *et al.*[22] The UA model treats the hydrocarbon groups as pseudoatoms, i.e., single interaction sites. For bonded interactions within a *n*-dodecane molecule, Nath *et al.* used the Khare *et al.* potential[23,24] to model the two-body bond stretching, the van der Ploeg and Berendsen potential[25] to model the three-body bond bending, and the Jorgensen potential[26] to model the four-body torsion. The non-bonded interactions between any two pseudoatoms that belong to the same molecule but are separated by more than three bonds are modeled by Lennard-Jones (LJ) potential with the parameters proposed by Smit *et al.*[27] The Smit *et al.* LJ potential is also used to model the interactions between pseudoatoms belonging to different molecules. The Lorentz–Berthelot (LB) mixing rule[28] is employed to determine the LJ parameters for interactions between CH_3 and CH_2 pseudoatoms. The cutoff distance for all LJ interactions is 13.8 Å.[22,27] This potential model has been shown to provide good agreement with the experimental

equilibrium for alkanes over a wide range of temperatures and chain lengths.[3–6,22,27]

For Au–Au interactions, we use the embedded-atom-method (EAM) potential.[29] The non-bonded interactions between Au and pseudoatoms in *n*-dodecane are also described by the LJ potential with parameters taken from the universal force field (UFF)[30] and calculated by the LB mixing rule. The same cutoff distance of 13.8 Å is used for the LJ interactions between Ar and *n*-dodecane. In all MD simulations, we use a velocity Verlet algorithm with multiple time steps[28] to integrate the equations of motions. A time step size of 1 fs is used for bond stretching, 2 fs is used for bond bending and torsion, and 4 fs is used for all other interactions.

B. The fluid properties of the model *n*-dodecane

Although the potential model used in this work provides generally better agreement with the experimental phase equilibrium data for *n*-dodecane than other models in the literature, recent MD simulation results[3–6] indicate that it is still not able to reproduce all fluid properties of *n*-dodecane found in the experiment with a high accuracy. For analysis of the evaporation/condensation and heat conduction across liquid–vapor interfaces of the model *n*-dodecane, therefore, we use equilibrium MD (EMD) simulations described in Secs. III B 1–III B 3 to determine the properties of the model *n*-dodecane including saturated vapor density, ρ_g, saturated liquid density, ρ_f, specific heat c_V, thermal conductivity, k, molecular mean free path (MFP), λ, and the MAC, α_M.

1. Determination of ρ_g and ρ_f

To determine the ρ_g and ρ_f of the model *n*-dodecane, we place a liquid slab of 5400 *n*-dodecane molecules in the middle of a simulation box, which has a length of 31.5 nm and a cross-sectional area of 15.0 × 15.0 nm^2. The box size is fixed during the simulation, and PBCs are applied in all three directions. We equilibrate the system at multiple temperatures varying from 400 K to 500 K using the Berendsen thermostat.[31] After the system reaches thermal equilibrium at each temperature, a liquid and vapor phase separated by two planar liquid–vapor interfaces is present in the same simulation cell, and the saturated vapor density, ρ_g, and the saturated liquid density, ρ_f, are calculated from the average density in the vapor phase and in the liquid phase, respectively. Figure 2 shows the representative MD simulation results at T = 450 K. If we define the liquid–vapor interfacial layer as the region whose density ranges from ρ_g+0.01ρ_f to 0.95ρ_f,[4,34] the result in Fig. 2 shows that the thickness of the interfacial layer at T = 450 K is ~2.6 nm, which is consistent with that found in the work of Xie *et al.* [4]

In Fig. 3, we compare the temperature-dependent saturated density determined in this work to the experimental data[32,33] and the results from the MD simulations[3,4] and the Monte Carlo (MC) simulations,[27] which used the same intermolecular potential as that in this work. Figure 3(a) shows that the ρ_f's found in our MD simulations are in good agreement with the experimental data and the results from the MD and MC simulations in the literature.

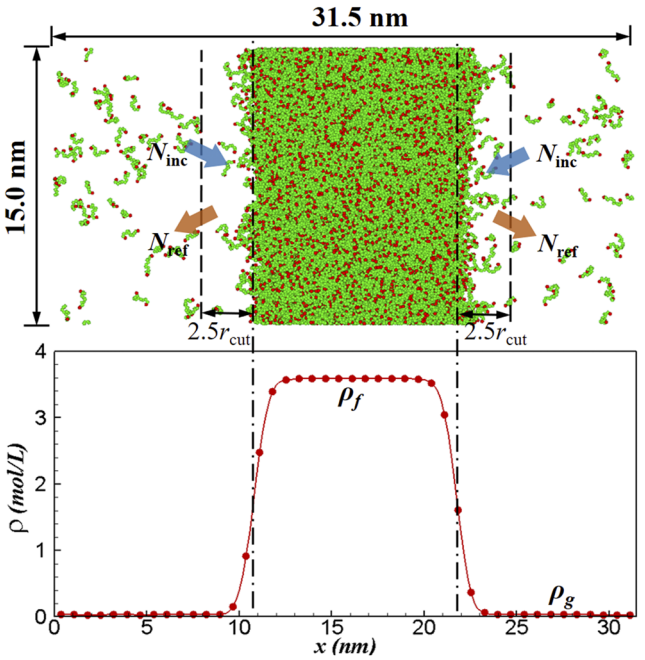

FIG. 2. A snapshot of the liquid–vapor coexistence system of the model *n*-dodecane at a temperature of 450 K and the corresponding density profile in the fluid system. The dashed–dotted lines indicate the position of liquid–vapor interfaces. The dashed lines indicate the position of imaginary planes used for the determination of the MAC. The solid line in the density profile is used as a guide to the eye.

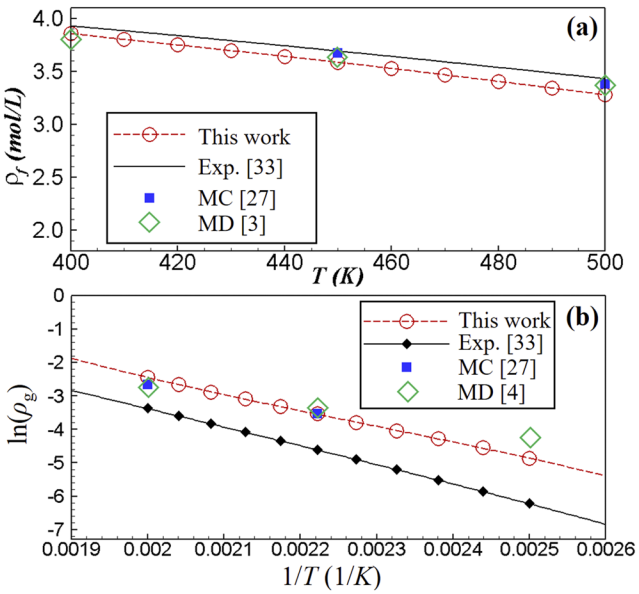

FIG. 3. (a) The saturated liquid density, ρ_f, of the model *n*-dodecane as a function of temperature. The dashed line in (a) is used as a guide to the eye. (b) ln(ρ_g) vs 1/T, where ρ_g is the saturated vapor density of the model *n*-dodecane. The dashed line and the solid line are the third order polynomial fit to the MD results in this work and to the experimental result, respectively.

Figure 3(b) shows that our simulation results of ρ_g are higher than the experimental data but in good agreement with the results from MD and MC simulations that used the same intermolecular potential. This suggests that the deviation between our MD results and the experimental data is not caused by the inaccuracy in our MD simulations, but by the imperfect potential model. The objective of this work is not to accurately reproduce the fluid properties of the real *n*-dodecane but to test the accuracy of various relationships in the prediction of the interfacial heat transfer rate for the model *n*-dodecane. Therefore, we will use the properties of the model *n*-dodecane in the subsequent analyses of thermal transport in the model *n*-dodecane.

To further verify that the temperature-dependent ρ_g found in our work is accurate for the model *n*-dodecane, we compare the simulation results to the prediction from the Clausius–Clapeyron equation.[35] If the ideal gas assumption is valid for the saturated vapor of the model *n*-dodecane, the temperature-dependent ρ_g satisfies [35]

$$\frac{d(\ln \rho_g)}{d(1/T)} = -\frac{h_{fg}}{R} + T, \tag{7}$$

where h_{fg} is the latent heat at a given temperature, T. To find h_{fg} of the model fluid, we carry out separate equilibrium MD simulations to determine the internal energy, u, and pressure, P, of the saturated liquid *n*-dodecane and the saturated vapor *n*-dodecane at a given temperature. Using the calculated u, P, and ρ, we determine the enthalpy, h_f, for the saturated liquid and the enthalpy, h_g, for the saturated vapor. The difference between the two enthalpies gives h_{fg} = 39.1 kJ/mol for the model fluid *n*-dodecane at T = 450 K.

In Fig. 3(b), we fit our $\ln(\rho_g)$ vs $1/T$ data with a third order polynomial and find that the local slope at T = 450 K is −4697 K, which has a reasonable agreement with −4257 K predicted by Eq. (7). Using the calculated P and ρ of the saturated vapor at T = 450 K, we find that the compressibility factor (CF) of the saturated vapor is 0.93, which implies that the saturated vapor of the model *n*-dodecane is close to, but not a perfect ideal gas at T = 450 K. Therefore, it is reasonable to see a ~10% difference between the MD result and the theoretical prediction. As a comparison, the compressibility factor of the saturated vapor of real *n*-dodecane at T = 450 K is 0.96.[32,33] The slope of $\ln(\rho_g)$ vs $1/T$ of the experimental data is −5644 K at T = 450 K, which deviates from −5275 K predicted from Eq. (7) by ~7%. Based on these results, we believe that our temperature-dependent ρ_g data are reliable in the analysis of the subsequent MD simulation results of evaporation and condensation processes.

2. Determination of c_V, k, and λ

For analysis of heat conduction across the liquid–vapor interface in MD simulations, it is important to evaluate the thermal conductivity, k, and the specific heat c_V, of the model *n*-dodecane. Additionally, we also evaluate the self-diffusion coefficient, D, which can be used to estimate the MFP of the *n*-dodecane molecules. All the aforementioned properties of the model *n*-dodecane at T = 450 K can be obtained from the output of a single EMD simulation.

In the EMD simulation, we place 2400 *n*-dodecane molecules in a cubic simulation cell such that the density of *n*-dodecane equals 0.029 mol/l, i.e., ρ_g of the model *n*-dodecane at T = 450 K. The box size is fixed during the simulation, and PBCs are applied in all three directions. We first equilibrate the system at T = 450 K using the Berendsen thermostat[31] for 3 ns. After the system reaches thermal equilibrium, the thermostat is turned off and an NVE simulation is carried out for 100 ns to determine k, c_V, and D of the model *n*-dodecane.

In a microcanonical ensemble, c_V can be calculated by[28]

$$\langle E_P^2 \rangle - \langle E_P \rangle^2 = \frac{d}{2} N k_B^2 T^2 \left(1 - \frac{dNk_B}{2c_V}\right), \tag{8}$$

where E_P is the total potential energy of the model system, $\langle \cdots \rangle$ denotes ensemble average, N is the number of molecules in the system, k_B is the Boltzmann constant, and d is the degree of freedom of each molecule. For the UA model used in this work, each *n*-dodecane molecule has 12 pseudoatoms, and thus, d = 36. Using Eq. (8) and the above-described EMD simulation, we find $c_{V,MD} = (35.3 \pm 0.1)R$, where R is the universal gas constant. This value is considerably lower than the experimental value $c_{V,exp} = 46.4R$[32,33] mainly because all vibrations associated with the C–H bonds in *n*-dodecane molecules are frozen in the UA model. The discrepancy between the MD simulation result and the experimental data cannot be eliminated by simply replacing the UA model with an all-atom model[36] because the accurate determination of c_V also needs to consider the quantum effects in molecular vibrations,[37,38] which are not taken into account in classical MD simulations.

Using the EMD simulation, we also determine k and D of the model *n*-dodecane from Green–Kubo formulas. The Green–Kubo formula for determination of D is given by[39]

$$D = \frac{1}{3} \int_0^\infty dt \langle \vec{v}_i(t) \cdot \vec{v}_i(0) \rangle, \tag{9}$$

where $\vec{v}_i$ is the center of mass (COM) velocity of molecule i and t is time. The Green–Kubo formula for determination of k is given by[39]

$$k = \frac{V}{3k_B T^2} \int_0^\infty dt \langle \vec{q}(t) \vec{q}(0) \rangle, \tag{10}$$

where V is the volume of the simulation box and q is the microscopic heat flux. For the model chain molecules in this work, we show in the Appendix that q can be computed from

$$\vec{q} = \frac{1}{V} \left(\sum_i \vec{v}_i E_i + \frac{1}{2} \sum_{i>j} \vec{r}_{ij} \left(\sum_{k \subset i, l \subset j} \vec{f}_{kl,\text{inter}} \cdot \left(\vec{v}_{a,k} + \vec{v}_{a,l} \right) \right) \right), \tag{11}$$

where E_i is the total energy (i.e., the sum of kinetic energy and potential energy) of molecule i, r_{ij} is the position vector from the COM of molecule j to the COM of molecule i, and the subscripts k and l represent pseudoatom k belonging to molecule i and pseudoatom l belonging to molecule j, respectively. In Eq. (11), $f_{kl,\text{inter}}$ is the interatomic force between pseudoatom k and pseudoatom l and $v_{a,k}$ and $v_{a,l}$ are the velocity of atom k and atom l, respectively.

To determine k and D of the model *n*-dodecane, we calculate the velocity autocorrelation function (VACF) in Eq. (9) and the heat flux autocorrelation function (HFACF) in Eq. (10). In Fig. 4, we show the MD simulation results of VACF, HFACF,

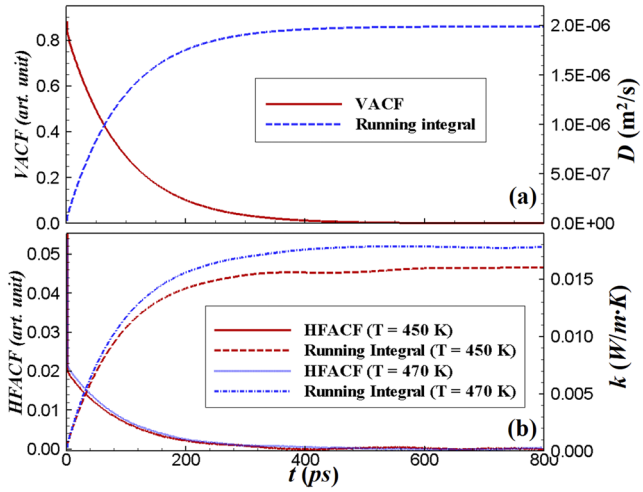

FIG. 4. (a) The VACF and its running integral for the model *n*-dodecane at ρ = 0.029 mol/l and T = 450 K, and (b) the HFACF and its running integral for the model *n*-dodecane at ρ = 0.029 mol/l and T = 450 K (red lines) and at ρ = 0.028 mol/l and T = 470 K (blue lines).

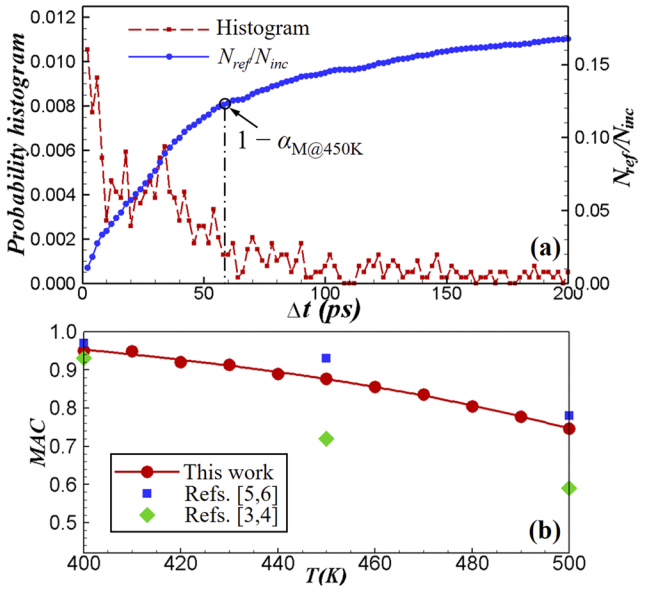

FIG. 5. (a) Probability of the return to the vapor histogram and its running integral N_{ref}/N_{inc} as a function of Δt at a temperature of 450 K. $1 - N_{ref}/N_{inc}$ at Δt = 58.3 ps is used to evaluate the MAC. (b) The MACs obtained in this work and from Refs. 3–6 as a function of temperature for the model *n*-dodecane. The dashed and solid lines in (a) are used as guides to the eye. The solid line in (b) is a third order polynomial fit to the MAC vs T in this work.

and their running integrals for the saturated vapor *n*-dodecane at T = 450 K. From the plateau of the running integral in Fig. 4(a), we obtain $D \approx 2 \times 10^{-6}$ m^2/s. Substituting this value in the Einstein–Smoluchowski equation,[12,40] we find that the MFP of the saturated model *n*-dodecane at T = 450 K is about 17 nm. From Fig. 4(b), we obtain k = 0.016 ± 0.001 W/m K for the saturated model *n*-dodecane at T = 450 K. Similar to the heat capacity result, the thermal conductivity found from the MD simulation is lower than the experimental value (0.021 W/m K[32,33]) mainly because the energy associated C–H bond vibration is not counted in the model *n*-dodecane. The calculated k is useful in the evaluation of conduction heat flux across the liquid–vapor interface in the subsequent non-equilibrium MD (NEMD) simulation.

3. Determination of α_M

Using the same MD model described in Sec. III B 1, we determine the MAC, α_M, which is defined as the fraction of vapor molecules that strike the liquid surface and are accommodated to the liquid phase. As shown in Fig. 2, we set an imaginary plane 3.45 nm (2.5 times of cutoff distance) from the liquid–vapor interface and define vapor molecules that pass through the imaginary plane and move toward the interface as incident molecules. In the 20-ns MD run, we follow the trajectory of each incident vapor molecule to determine the time interval, Δt, for each incident molecule to pass through the imaginary plane again and return to the vapor phase. The distance between the imaginary plane and the interface is greater than the thickness (~2.6 nm) of the liquid–vapor interfacial layer to ensure that the reflected molecules are out of the interface and is much smaller than the MFP (~17 nm) of vapor molecules to ensure that the incident molecules mainly collide/interact with the liquid surface, not with other vapor molecules.

In Fig. 5(a), we show the probability histogram of Δt for the model *n*-dodecane molecules returning to the vapor phase at a temperature of 450 K. The time interval, Δt, for vapor molecules that are directly reflected by the liquid surface will be smaller than that for vapor molecules that are first accommodated to the liquid phase and later evaporated. To determine if the incident molecule is accommodated to the liquid surface, therefore, one needs to find a cutoff time interval, Δt_{cut}. Near a liquid–vapor interface at equilibrium, the average molar flux of vapor molecules striking the liquid–vapor interface is $\rho_v RT_v/2\pi M$.[12] Since only half of vapor molecules move toward the interface and another half move away from the interface, the average normal velocity, v_n, of incident vapor molecules is $2RT_v/\pi M$. Accordingly, for incident molecules that were directly reflected by the interface, the average time interval should be $\Delta t_{avg} = 2\Delta x/v_n$, where Δx is the distance between the imaginary plane and the liquid–vapor interface. For vapor *n*-dodecane at T = 450 K, v_n = 118.3 m/s and Δt_{avg} = 58.3 ps.

Using 58.3 ps as the cutoff time interval, we show in Fig. 5(a) that the Δt_{cut} divides the histogram into two regimes: one with high and rapidly declining values and the other with low and slowly declining values. The second regime is related to the events when vapor molecules incoming to the liquid–vapor interface are first accommodated and later evaporated. To determine the MAC, therefore, we integrate the histogram from Δt = 0 to Δt = 58.3 ps and use the integral to evaluate the total probability of direction reflection, N_{ref}/N_{inc}, where N_{inc} is the number of incident molecules and N_{ref} is the total number of incident molecules that are directly reflected. The MAC is determined by $\alpha_M = 1 - N_{ref}/N_{inc}$. Using this approach, we find α_M = 0.88 ± 0.01 for the model *n*-dodecane at T = 450 K. For MACs at other temperatures, we use the Δt_{cut} corresponding

TABLE I. The specific heat, c_V, thermal conductivity, k, self-diffusion coefficient, D, molecular MFP, λ, compressibility factor, CF, and density, ρ_g, of the model saturated vapor n-dodecane at T = 450 K. The latent heat, h_{fg}, and the MAC, α_M, of the model n-dodecane at T = 450 K. All results are obtained from MD simulations described in Sec. III.

c_V (R)	k (W/m K)	D (m^2/s)	λ (nm)	h_{fg} (kJ/mol)	α_M	CF	ρ_g (mol/l)	$d\rho_g/dT$ (mol/l K)
35.3	0.016	2.0×10^{-6}	17	39.13	0.88	0.93	0.029	6.62×10^{-4}

to the average flight time at a given temperature to evaluate the corresponding MAC.

In Fig. 5(b), we compare our MD simulation results of the temperature-dependent MAC to those in the literature.[3–6] The previous and present MD simulation results all show that the MAC decreases with an increase in temperature. The MACs from our work are generally higher than those in the work of Cao, Xie, and Sazhin.[3,4] The difference might be associated with the much smaller simulation cell used in the work of Cao, Xie, and Sazhin.[3,4] The more recent MD simulation results by Nagayama *et al.*[5,6] exhibit a much better agreement with our results. In our previous work,[17] we used the similar method to calculate the MAC of a model fluid Ar at various temperatures and found that the MACs obtained from our EMD simulations agree well with those obtained from NEMD simulations.[41] These results imply that the MD method used in this work is robust and reliable in the determination of MAC. The MACs obtained in this section will be used in the analysis of evaporation and condensation processes in Sec. IV.

For the convenience of discussions of simulation results in Secs. IV and V, we summarize all properties of the model n-dodecane at T = 450 K obtained in this section in Table I.

IV. NEMD SIMULATION OF EVAPORATION AND CONDENSATION

A. NEMD simulation details

To study evaporation and condensation of the model n-dodecane, we first equilibrate the fluid and the solid shown in Fig. 1 at a temperature of 450 K for 4 ns with the Berendsen thermostat.[31] The thermostat in the fluid is then turned off, and the system is equilibrated at a temperature of 450 K for another 4 ns. After equilibration, the density of vapor in the central vapor region is 0.029 ± 0.001 mol/l, which is consistent with ρ_g = 0.029 mol/l found in Sec. III B 1. This indicates that the thickness of the liquid film in the model system is large enough to avoid the effects of disjoining pressure on the equilibrium properties of the model n-dodecane. In Sec. III B 2, we find that the MFP of the saturated model n-dodecane at T = 450 K is about 17 nm. Accordingly, the Knudsen number in the vapor phase of the model system is about 0.17.

Subsequently, we set the left Au slab as the heat source and the right Au slab as the heat sink. This results in evaporation of n-dodecane on the left surface and condensation of n-dodecane on the right surface. The heat source temperature, T_h, and the heat sink temperature, T_l, are maintained in the subsequent MD simulations by velocity rescaling[42] at each time step. Each heat source–sink simulation run is first carried out for 4 ns to allow the system to reach quasi-steady-state evaporation and condensation and then for additional 4 ns for data collection and averaging. We consider the simulated process as a quasi-steady-state evaporation and condensation process since the moving speed of liquid–vapor interfaces is more than 100 times slower than the bulk velocity of vapor.

To calculate the steady-state temperature and density profiles, we evenly divide the fluid region less than 12 nm from each of the two solid surfaces into ten bins. The 1.2-nm bin width in this region allows us to find the location and temperature of the liquid surface with precision. In the 96-nm-long central vapor region, we evenly divide the region into eight bins. The 12-nm bin width in the central vapor region allows us to obtain good statistics of vapor properties. The steady-state evaporation/condensation molar flux is determined by $J_{MD} = \Sigma v_{i,x}/(VN_A)$, where N_A is the Avogadro constant and V and $v_{i,x}$ are the volume and the x-component velocity of n-dodecane molecules in the central vapor region, respectively. The contribution from the macroscopic velocity is subtracted in the calculation of temperature in each bin. To further improve the accuracy of the simulation results, four independent runs are performed in each case of MD simulations. The uncertainties of the simulation results are determined by analyses of these independent runs.

B. Representative simulation results

The representative NEMD simulation results in the case of T_h = 490 K and T_l = 410 K are shown in Fig. 1. One can see from Figs. 1(a) and 1(b) that the temperature and density in the central vapor region are almost constant. This indicates that the heat conduction and mass diffusion in the vapor region are negligible. In this case, the transport of thermal energy and mass at the two liquid–vapor interfaces is dominated by evaporation and condensation. From the NEMD simulation, we directly obtain the steady-state evaporation/condensation flux J_{MD} = 0.142 ± 0.008 mol/cm^2 s.

To compare J_{MD} with the prediction from the Schrage relationships, we first find the temperature at the two liquid surfaces. As shown in Fig. 1, we consider that the liquid surface is located at the bin where the fluid density starts to drop abruptly. Accordingly, we find the temperature at the left liquid surface $T_{L,1}$ = 471.2 K and that at the right liquid surface $T_{L,2}$ = 427.1 K, as shown in Fig. 1(b). Using $T_{L,1}$, $T_{L,2}$, and the ρ_g vs T data found in Sec. III B 1, we obtain $\rho_g(T_{L,1})$ = 0.0464 mol/l and $\rho_g(T_{L,2})$ = 0.0167 mol/l. Furthermore, using the α_M vs T data obtained in Sec. III B 3, we obtain $\alpha_M(T_{L,1})$ = 0.83 and $\alpha_M(T_{L,2})$ = 0.92. Additionally, we obtain ρ_v = 0.0280 mol/l and T_v = 462.0 K directly from the results in Fig. 1. All these properties are summarized in Table II. With the above properties, Eq. (1), i.e., the Schrage relationship, predicts the net evaporation flux at the left surface, $J_{net,evp}$ = 0.146 mol/cm^2 s, and the net condensation flux at the right surface, $J_{net,con}$ = 0.137 mol/cm^2 s.

TABLE II. Comparison of the molar fluxes obtained from MD simulations with the predictions from the Schrage relationships. $J_{net,evp}$ and $J_{net,con}$ are evaporation and condensation molar fluxes predicted by Schrage relationships, respectively. Error % is defined as $|J_{th} - J_{MD}|/J_{MD}$.

T_h (K)	T_l (K)	$T_{L,1}$ (K)	$T_{L,2}$ (K)	$\bar{T}_L$ (K)	T_v (K)	ρ_v (mol/l)	J_{MD} (mol/cm^2 s)	$J_{net,evp}$ (mol/cm^2 s)	$J_{net,con}$ (mol/cm^2 s)	Error % Evp.	Con.
460	440	454.7	443.1	448.9	450	0.0285	0.038 ± 0.006	0.031	0.041	18.4	7.9
470	430	459.9	437.8	448.9	453	0.0279	0.073 ± 0.008	0.070	0.070	4.1	4.1
480	420	464.3	431.9	448.1	458	0.0275	0.108 ± 0.013	0.101	0.102	6.5	5.6
490	410	471.2	427.1	449.2	462	0.0280	0.142 ± 0.008	0.146	0.137	2.8	3.5
500	400	476.5	421.7	449.1	463	0.0283	0.190 ± 0.011	0.183	0.174	3.7	8.4

Both of them agree with J_{MD} = 0.142 ± 0.008 mol/cm^2 s very well.

To provide further insight into the accuracy of the Schrage relationship in the prediction of evaporation and condensation fluxes of the model *n*-dodecane, we note that a key assumption made in the derivation of Schrage relationships is that the vapor molecules adjacent to the evaporating/condensing interfaces have a Maxwell velocity distribution (VD) shifted by the mean velocity of vapor, $v_{v,0}$. In our previous work,[17] we have shown that this assumption is accurate in the case of evaporation/condensation of monatomic fluids. To test if the assumption is also valid for evaporation/condensation of *n*-dodecane, we calculate the VD of vapor molecules in the leftmost (i.e., closest to the evaporating surface) and rightmost (i.e., closest to the condensing surface) bins of the central vapor region. If the assumption made in Schrage's analysis is valid, the steady-state VD obtained directly from the MD simulation should follow the shifted Maxwell velocity distribution (SMVD), given by[11]

$$f(v_x) = \sqrt{\frac{M}{2\pi R T_v}} e^{-\frac{M(v_x - v_{v,0})^2}{2RT_v}}. \quad (12)$$

As shown in Fig. 6, the VDs obtained directly from MD simulation closely follow the SMVD given by Eq. (12). Hence, the key Schrage assumption is still valid in the case of steady-state evaporation/condensation of *n*-dodecane. This explains why the Schrage relationships are also accurate in the prediction of steady-state evaporation and condensation fluxes of *n*-dodecane.

C. Effects of temperature difference on *J*

Using a similar methodology described in Secs. IV A and IV B, we study how evaporation and condensation fluxes vary with the temperature difference between the two liquid surfaces. In all cases, T_h and T_l are higher and lower than 450 K by the same amount, respectively. As a result, Table II shows that the average of the two liquid surface temperatures, $\bar{T}_L = (T_{L,1} + T_{L,2})/2$, is always close to 450 K. In each case, we obtain the evaporation/condensation molar flux, J_{MD}, directly from MD simulations and compare J_{MD} with the predictions from the Schrage relationship. Since the key Schrage assumption regarding the VD of vapor molecules near the evaporating and condensing surfaces is still valid for *n*-dodecane, it is reasonable to see in Table II that J_{MD} is in good agreement with the predictions from the Schrage relationship in all simulated cases.

The driving force for the evaporation and condensation processes in the model system is the temperature difference, $\Delta T_L = T_{L,1} - T_{L,2}$, between the two liquid surfaces. As ΔT_L varies from 11.6 K to 54.8 K, J_{MD} increases from 0.036 mol/cm^2 s to 0.190 mol/cm^2 s. Figure 7 shows that J_{MD} increases almost linearly with an increase in ΔT_L when ΔT_L is less than 45 K (i.e., 10% of $\bar{T}_L$). The linear fit to the data in Fig. 7 has a slope of ~0.0032 mol/cm^2 s K. In our previous work,[17] a similar linear dependence of J_{MD} on ΔT_L is also found in a monatomic fluid system. To understand the linear dependence of J_{MD} on ΔT_L in the model *n*-dodecane system, we carry out a similar analysis as we did in the monatomic fluid system. We have shown that the Schrage relationship is accurate in the prediction of

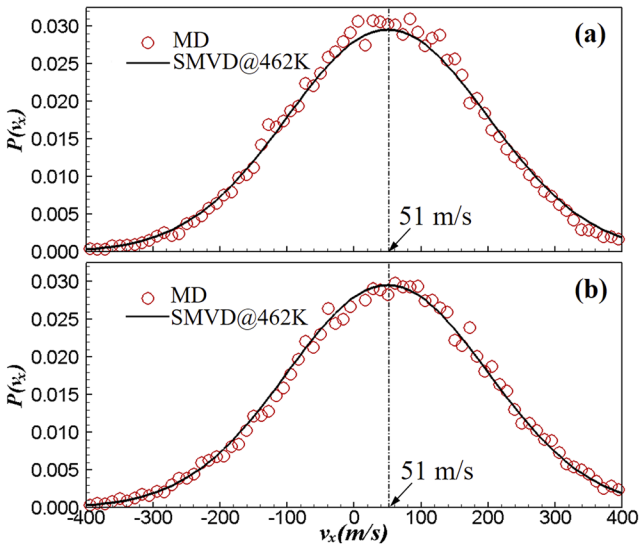

FIG. 6. The steady-state x-component VD of vapor molecules in the (a) leftmost bin (closest to the evaporating surface) and (b) rightmost bin (closest to the condensing surface) of the central gas region in the case of T_h = 490 K and T_l = 410 K. The scatters are VDs obtained directly from MD simulations. The lines are the SMVD given by Eq. (12). The vertical dashed–dotted lines show the mean velocity of vapor molecules.

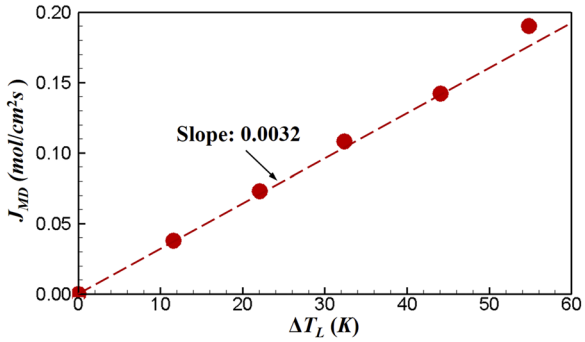

FIG. 7. J_{MD} as a function of ΔT_L. The dashed line shows the linear fit to J_{MD} vs ΔT_L when ΔT_L is less than 45 K. The uncertainty of J_{MD} is smaller than the size of symbols.

evaporation and condensation rates of *n*-dodecane. In the limit of a small driving force, the Schrage relationship can be approximated to[11,13]

$$J_{net,evp} \approx \frac{2\alpha_M(T_{L,1})}{2-\alpha_M(T_{L,1})}\sqrt{\frac{R}{2\pi M}}\left(\rho_g(T_{L,1})\sqrt{T_{L,1}}-\rho_v\sqrt{T_v}\right) \quad (13)$$

for the net evaporation flux on the left liquid surface and to

$$J_{net,con} \approx \frac{2\alpha_M(T_{L,2})}{2-\alpha_M(T_{L,2})}\sqrt{\frac{R}{2\pi M}}\left(\rho_v\sqrt{T_v}-\rho_g(T_{L,2})\sqrt{T_{L,2}}\right) \quad (14)$$

for the net condensation flux on the right liquid surface. For steady-state evaporation and condensation processes, we show in Sec. IV B that the temperature and density in the central vapor region are almost constant. Using $J_{net,evp} = J_{net,con}$ at steady state and the approximation $\alpha_M(T_{L,1}) \approx \alpha_M(T_{L,2}) \approx \alpha_M(\bar{T}_L)$, the average of Eqs. (13) and (14) is given by

$$J = \frac{\alpha_M(\bar{T}_L)}{2-\alpha_M(\bar{T}_L)}\sqrt{\frac{R}{2\pi M}}\left(\rho_g(T_{L,1})\sqrt{T_{L,1}}-\rho_g(T_{L,2})\sqrt{T_{L,2}}\right). \quad (15)$$

Using the Taylor expansion in Eq. (15) in the limit of $\Delta T_L/\bar{T}_L \ll 1$, which is the case in our modeling results, one can prove that $J/\Delta T_L$ is given by[17]

$$\frac{J}{\Delta T_L} \approx \frac{\alpha_M(\bar{T}_L)}{2-\alpha_M(\bar{T}_L)}\sqrt{\frac{R}{2\pi m\bar{T}_L}}\rho_g(\bar{T}_L)\left(\frac{\bar{T}_L}{\rho_g(\bar{T}_L)}\left.\frac{d\rho_g}{dT}\right|_{\bar{T}_L}+\frac{1}{2}\right). \quad (16)$$

If the ideal gas approximation of the vapor is valid, one can use the Clausius–Clapeyron equation to further reduce Eq. (16) to[17]

$$\frac{J}{\Delta T_L} \approx \frac{\alpha_M(\bar{T}_L)}{2-\alpha_M(\bar{T}_L)}\sqrt{\frac{R}{2\pi m\bar{T}_L}}\rho_g(\bar{T}_L)\left(\frac{h_{fg}(\bar{T}_L)}{R\bar{T}_L}-\frac{1}{2}\right). \quad (17)$$

Note that all properties on the right-hand side of Eqs. (16) and (17) are evaluated at $\bar{T}_L$. This indicates that the evaporation/condensation flux, J, will increase linearly with ΔT_L if the average liquid surface temperature, $\bar{T}_L$, remains constant as ΔT_L increases.

One can see in Table II that $\bar{T}_L$ of all simulated cases is close to 450 K. Using $\alpha_M(450\ \text{K}) = 0.88$, $\rho_g(450\ \text{K}) = 0.029$ mol/l, and $d\rho_g/dT|_{450K} = 6.62 \times 10^{-4}$ mol/l K found in Sec. III, Eq. (16) predicts $J/\Delta T_L = 0.0032$ mol/cm^2 s K, which is in excellent agreement with the slope found in Fig. 7. When ΔT_L is greater than 45 K (i.e., 0.1 $\bar{T}_L$), Fig. 7 shows that the nonlinear effects become visible and J_{MD} vs ΔT_L starts to deviate from the linear relation. Furthermore, using the property $h_{fg}(450\ \text{K}) = 39.13$ kJ/mol found in Sec. III, Eq. (17) predicts $J/\Delta T_L = 0.0030$ mol/cm^2 s K, which deviates slightly from the slope in Fig. 7. Since Eq. (17) is only valid for ideal gases and the compressibility factor of the saturated model *n*-dodecane at $T = 450$ K is 0.93, we believe that the small deviation in the prediction of Eq. (17) is associated with the non-ideal behavior of the model vapor.

V. NEMD SIMULATION OF INTERFACIAL HEAT CONDUCTION

A. NEMD simulation details

The model system used in the study of interfacial heat conduction is similar to that in the study of evaporation and condensation processes. The main difference is that there is no liquid layer (except for an adsorbed layer that will not evaporate in the simulation) on the hot solid surface, as shown in Fig. 8. Accordingly, there will be no evaporation on the hot surface, and the mass flux in the model system must be zero at steady state. In this case, the steady-state heat transfer across the liquid–vapor interface is by conduction only. In the diesel engine-like conditions,[1,2] the diesel fuel is sprayed into hot gas. Using the model system shown in Fig. 8, we mimic heat conduction from hot gas to liquid *n*-dodecane.

In NEMD simulations, energy is added at a constant rate of 1.32 nW to the left solid surface and is removed at the same rate

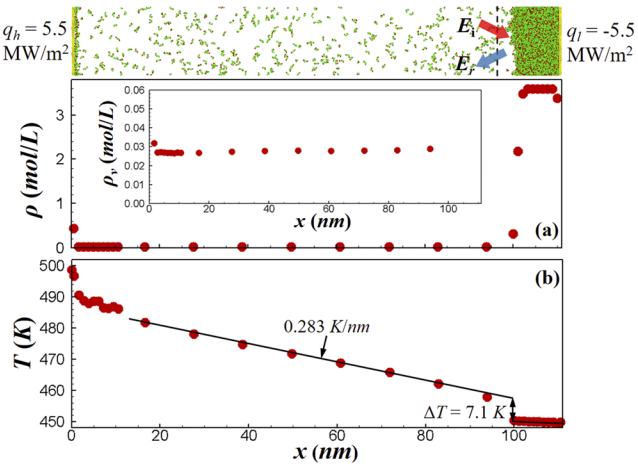

FIG. 8. (Top panel) A snapshot of the model system for the study of heat conduction across the liquid–vapor interface of the model *n*-dodecane. The dashed line indicates the position of the imaginary plane. (Bottom panels) (a) Density and (b) temperature profiles at steady state. The inset in (a) shows the density profile in the vapor phase. The two solid lines in (b) are the linear fit to the temperature profile in the vapor phase and in the liquid phase, respectively.

from the right solid surface at each time step by velocity rescaling.[42] This results in a constant heat flux of 5.5 MW/m^2 across the liquid–vapor interface at steady state. Each heat source–sink simulation run is first carried for 6 ns to allow the system to reach a steady state, and then, it is run for an additional 6 ns for data collection and averaging. Four independent runs are carried out to further improve the accuracy of the simulation results. To avoid a too large temperature jump at the interface between the vapor and the left solid surface, we doubled the interaction strength between Au and *n*-dodecane molecules. Such a modification will not affect the simulation results on the thermal conductance at the liquid–vapor interface.

To predict the interfacial thermal conductance from the KTG, one needs to know the TAC of vapor molecules at the model surface. To determine the TAC defined in Eq. (5), we set an imaginary plane 3.45 nm from the liquid surface, as shown in Fig. 8. The distance between the plane and the surface is greater than the thickness of the liquid–vapor interfacial layer and much smaller than the MFP of vapor molecules. The vapor molecules passing through the imaginary plane are defined as incident or reflected molecules depending on their instantaneous COM velocity directions. This procedure is similar to that in the determination of the MAC in Sec. III B 3. The simulation results are shown in Sec. V B.

B. Conduction heat flux across the liquid–vapor interface

1. The representative results

As described in Sec. V A, we directly applied a constant heat flux of 5.5 MW/m^2 across the liquid–vapor interface in the NEMD simulation. To understand the heat conduction at the liquid–vapor interface from the KTG, we first find the steady-state temperature and density profiles in the model system. As shown in Fig. 8(b), the temperature in the vapor phase decreases almost linearly in the heat flow direction with a slope of 0.283 K/nm, indicating evident heat conduction in the vapor phase. With the heat flux and the temperature gradient obtained directly from the NEMD simulation, the Fourier law predicts that the thermal conductivity of the model *n*-dodecane vapor in the model system is ~0.019 W/m K. At the center of the vapor phase, the temperature and density are 470 K and 0.028 mol/l, respectively. Using the EMD method described in Sec. III B 2, we show in Fig. 4(b) that the thermal conductivity of the model *n*-dodecane at 470 K and 0.028 mol/l is 0.018 ± 0.001 W/m K. The good agreement between the EMD and NEMD results validates the thermal conductivity obtained from our EMD simulations.

To obtain the prediction of interfacial thermal conductance, G_K, from Eq. (6), we first find from Fig. 8 that the temperature and density of vapor near the liquid–vapor interface are 457.3 K and 0.028 mol/l, respectively. Substituting these two values into Eq. (4), we obtain that N_{gas} equals to 0.167 mol/cm^2 s. Furthermore, we find from Fig. 8 that the liquid surface temperature is 450.2 K. At T_s = 450.2 K, we obtain that c_V in Eq. (6) is ~35.3R from the EMD simulation described in Sec. III B 2. The TAC, α_T, in Eq. (6) is determined by Eq. (5). As shown in Fig. 9(a), we obtain the time-averaged energy of incident (E_i) and reflected (E_r) vapor molecules at steady state. To determine E_s, i.e., the average energy

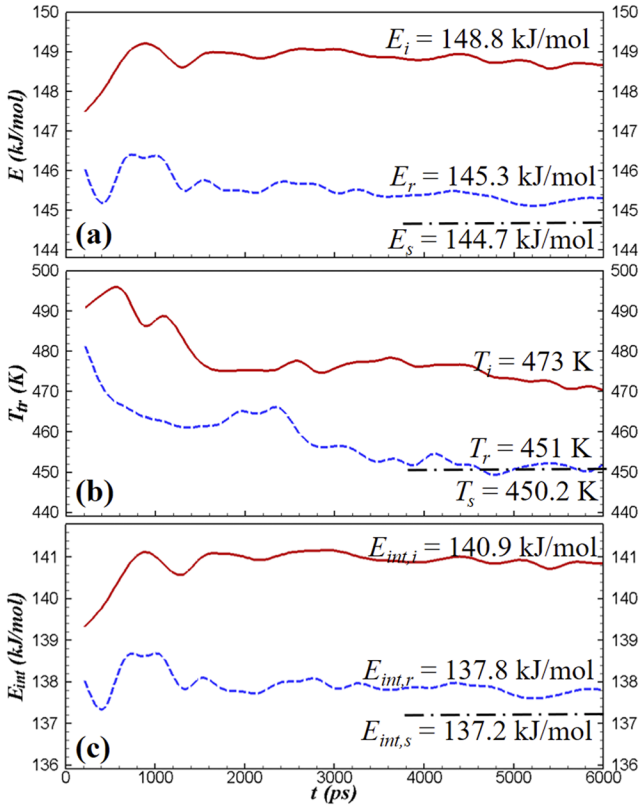

FIG. 9. (a) The time-averaged energy of incident (solid line) and reflected (dashed line) vapor molecules. The horizontal dashed–dotted line represents the average energy a gas would carry if it equilibrates with the liquid surface upon reflection. (b) The time-averaged translational temperature of incident (T_i, solid line) and reflected (T_r, dashed line) vapor molecules. The horizontal dashed–dotted line indicates the liquid surface temperature, T_s. (c) The time-averaged energy of internal motions of incident (solid line) and reflected (dashed line) vapor molecules. The horizontal dashed–dotted line represents the average energy of internal motions a gas would carry if it equilibrates with the liquid surface upon reflection.

a gas would carry if it equilibrates with the liquid surface upon reflection, we equilibrate the liquid–vapor coexistence system at T_s = 450.2 K and determine the average energy, E_v, of the vapor that is in equilibrium with the liquid. E_s is determined by $E_v + \frac{1}{2} RT_s$, where $\frac{1}{2} RT_s$ is the streaming correction[12] to the reflected gas energy. From the calculated E_i, E_r, and E_s shown in Fig. 9(a), we obtain α_T = 0.85.

To understand how internal motions of *n*-dodecane molecules affect the TAC, we further divide the molecular energy (E) into the energy of molecular translational motions (E_{tr}) and the energy of molecular internal motions (E_{int}), i.e., molecular rotations and vibrations. E_{tr} of incident ($E_{tr,i}$) and reflected ($E_{tr,r}$) vapor molecules can be determined directly from molecular translational velocity. The translational energy of incident and reflected vapor molecules divided by 2R gives the translational temperature of incident and reflected molecules.[12] Since $E = E_{tr} + E_{int}$, we obtain $E_{int,i}$ and $E_{int,r}$ in Fig. 9(c) from $E_i - E_{tr,i}$ and $E_r - E_{tr,r}$, respectively. Moreover, $E_{int,s}$ in Fig. 9(c) is determined from $E_s - 2RT_s$. Using E_{tr} and E_{int} in Eq. (5),

we can determine the TAC of translational motions ($\alpha_{T,\mathrm{tr}}$) and that of internal motions ($\alpha_{T,\mathrm{int}}$) from MD simulations.

In our previous work,[15] we found that the TAC of vapor Ar molecules, which have only translation motions, is close to unity on the liquid Ar surface. Figure 9(b) shows that the translational temperature of reflected vapor *n*-dodecane molecules is very close to the liquid surface temperature, which means $\alpha_{T,\mathrm{tr}}$ is also close to unity for *n*-dodecane. By comparison, $\alpha_{T,\mathrm{int}}$ of *n*-dodecane is about 0.84. In our previous study on the TAC of gas molecules on solid surfaces,[21] we also found that the molecular internal motions are more difficult to thermalize with surfaces than translational motions. Therefore, the MD simulation results indicate that the incomplete energy exchange ($\alpha_T = 0.85$) between *n*-dodecane vapor and its own liquid is mainly due to the relatively lower TAC of molecular internal motions.

With the calculated N_{gas}, c_V, and α_T, Eq. (6) predicts that $G_K = 0.73$ MW/m^{2}K. To test the accuracy of this prediction, we compare it to the G_K obtained directly from the NEMD simulation. By extrapolating the linear fit of the temperature profile in the vapor and liquid phases to the liquid–vapor interface, we obtain that the temperature jump, ΔT, at the liquid–vapor interface is 7.1 ± 0.3 K. Using the constant heat flux (5.5 MW/m^2) applied in the NEMD simulation and $\Delta T = 7.1 \pm 0.3$ K, we obtain $G_K = 0.77 \pm 0.03$ MW/m^{2}K, which validates the prediction from the kinetic theory based Eq. (6).

2. Verification of Eq. (6) at a lower temperature

Using the similar method, we calculate G_K at the model *n*-dodecane liquid surface at a lower temperature (T_s = 429.5 K) by applying a constant heat flux (4.9 MW/m^2) across the liquid–vapor interface. From the NEMD simulation, we first obtain $\alpha_T = 0.90$, which is higher than $\alpha_T = 0.85$ at T_s = 450.2 K. The higher α_T at the lower temperature is associated with the higher α_M at the lower temperature found in Sec. III B 3. The higher α_M indicates that more incident vapor molecules are accommodated to the liquid phase before they return to the vapor phase. Accordingly, the vapor molecules have a higher possibility to have complete energy exchange with the liquid surface upon reflection.

As shown in Fig. 10, the temperature at the center of the vapor phase is about 450 K. With the heat flux (4.9 MW/m^2) and the temperature gradient (0.3 K/nm) obtained directly from the NEMD simulation, the Fourier law predicts that the thermal conductivity of the model *n*-dodecane vapor is ~0.016 W/m K. The NEMD prediction is again consistent with the EMD prediction $k = 0.016 \pm 0.001$ W/m K found in Sec. III B 2 at a temperature of 450 K. With the TAC, temperature, density, and specific heat of the vapor obtained from MD simulations, Eq. (6) predicts $G_K = 0.48$ MW/m^{2}K at the liquid *n*-dodecane surface at $T_s = 429.5$ K. The lower G_K value compared to that at T_s = 450.2 K is caused by the much lower vapor density near the low temperature surface, which results in a lower frequency of collisions between vapor molecules and the liquid surface. To verify the G_K predicted by the KTG, we find the temperature jump, $\Delta T = 9.6 \pm 0.4$ K, at the liquid–vapor interface directly from the NEMD simulation. Accordingly, the G_K directly obtained from the NEMD simulation is 0.51 ± 0.02 MW/m^{2}K, which is again consistent with the prediction from the KTG.

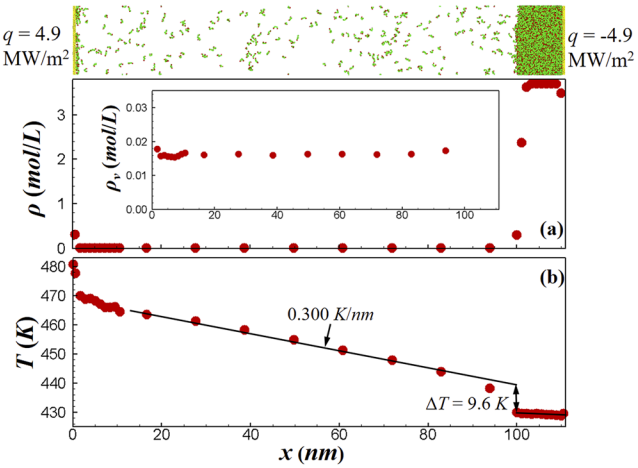

FIG. 10. Same as in Fig. 8 except that q = 4.9 MW/m^2 and liquid surface temperature T_s = 429.5 K.

VI. SUMMARY AND CONCLUSIONS

Using MD simulations, we studied the thermal transport across the liquid–vapor interface of the model *n*-dodecane. Two thermal transport mechanisms, namely, evaporation and heat conduction, often occur simultaneously at evaporating liquid surfaces. To have a good understanding of each thermal transport mechanism, we restrict the thermal energy to be transferred across the liquid–vapor interface by one mechanism in each NEMD run. The MAC and TAC of the model *n*-dodecane, which are important properties for the understanding of evaporation and interfacial heat conduction processes, are determined from MD simulations with high fidelity. The simulation results are discussed in the context of the kinetic theory based analysis.

In the case of interfacial thermal transport by evaporation/condensation, our simulation results show that the key assumption in Schrage's analysis regarding the VD of vapor molecules near the evaporating/condensing interfaces is still valid for the fluids containing chain molecules such as *n*-dodecane. The Schrage relationship, which is accurate in the prediction of evaporation and condensation rates for monatomic fluids, also gives a good prediction of the steady-state evaporation and condensation rates for the model *n*-dodecane. Hence, our modeling results show that the validity and accuracy of the Schrage relationship are not affected by the complex molecular structure or inter-/intra-molecular interactions in *n*-dodecane.

The key problem in the prediction of heat conduction rates at liquid–vapor interfaces is to determine the thermal conductance, G_K, at the interface. The KTG predicts that the G_K at liquid–gas interfaces is determined by the frequency of collisions between gas molecules and the liquid surface, and the TAC. The MD simulation results show that the molecular internal motions are more difficult to thermalize with liquid surfaces than translational motions. With the accurate TAC obtained from the MD simulation, the kinetic theory based equation [i.e., Eq. (6)] is accurate in the prediction of the G_K at the liquid–vapor interface of the model *n*-dodecane.

ACKNOWLEDGMENTS

This work was supported by the NSF CBET Thermal Transport Processes Program under Grant No. 1911433. Additionally, we would like to thank the eXtreme Science and Engineering Discovery Environment (XSEDE) for providing us supercomputer resources for MD simulations.

APPENDIX: THE EXPRESSION FOR MICROSCOPIC HEAT FLUX OF THE MODEL CHAIN MOLECULE

The microscopic heat flux of a pure fluid is determined by[39]

$$\vec{q} = \frac{1}{V}\left(\sum_i \vec{v}_i E_i + \sum_i \vec{r}_i \frac{dE_i}{dt}\right), \tag{A1}$$

where r_i is the center of mass position of molecule i. For the model chain molecule, the total energy of molecule i is given by

$$E_i = \left(\sum_{k\subset i} \tfrac{1}{2} m_k \vec{v}_{a,k}^{\,2}\right) + V_{\text{intra},i} + \sum_{\substack{k\subset i, l\subset j \\ i\neq j}} V_{\text{inter},kl}, \tag{A2}$$

where the first, second, and third terms on right-hand side represent the total kinetic energy, the total intramolecular potential energy, and the total intermolecular energy of molecule i, respectively. Accordingly, dE_i/dt in Eq. (A1) can be computed from

$$\begin{aligned}
\frac{dE_i}{dt} &= \left(\sum_{k\subset i} m_k \vec{v}_{a,k} \frac{d\vec{v}_{a,k}}{dt}\right) + \left(\sum_{k\subset i} \frac{\partial V_{\text{intra}}}{\partial \vec{r}_k}\frac{d\vec{r}_k}{dt}\right) + \tfrac{1}{2}\sum_{\substack{k\subset i, l\subset j \\ i\neq j}} \frac{\partial V_{kl,\text{inter}}}{\partial \vec{r}_{kl}}\frac{d\vec{r}_{kl}}{dt} \\
&= \left(\sum_{k\subset i} \vec{v}_{a,k}\vec{f}_k\right) - \left(\sum_{k\subset i} \vec{v}_{a,k}\vec{f}_{k,\text{intra}}\right) - \tfrac{1}{2}\sum_{\substack{k\subset i, k\subset j \\ i\neq j}} \vec{f}_{kl,\text{inter}}\left(\vec{v}_{a,k} - \vec{v}_{a,l}\right) \\
&= \left(\sum_{k\subset i} \vec{v}_{a,k}\vec{f}_{k,\text{inter}}\right) - \tfrac{1}{2}\sum_{\substack{k\subset i, k\subset j \\ i\neq j}} \vec{f}_{kl,\text{inter}}\left(\vec{v}_{a,k} - \vec{v}_{a,l}\right) \\
&= \tfrac{1}{2}\sum_{\substack{k\subset i, l\subset j \\ i\neq j}} \vec{f}_{kl,\text{inter}}\left(\vec{v}_{a,k} + \vec{v}_{a,l}\right).
\end{aligned} \tag{A3}$$

Using Eq. (A3), the second summation in Eq. (A1) can be calculated by

$$\begin{aligned}
\sum_i \vec{r}_i \frac{dE_i}{dt} &= \sum_i \vec{r}_i \left(\tfrac{1}{2}\sum_{\substack{k\subset i, l\subset j \\ i\neq j}} \vec{f}_{kl,\text{inter}}\left(\vec{v}_{a,k} + \vec{v}_{a,l}\right)\right) \\
&= \tfrac{1}{4}\sum_i \vec{r}_i \left(\sum_{\substack{k\subset i, l\subset j \\ i\neq j}} \vec{f}_{kl,\text{inter}}\left(\vec{v}_{a,k} + \vec{v}_{a,l}\right)\right) \\
&\quad + \tfrac{1}{4}\sum_j \vec{r}_j \left(\sum_{\substack{k\subset i, l\subset j \\ i\neq j}} \vec{f}_{kl,\text{inter}}\left(\vec{v}_{a,k} + \vec{v}_{a,l}\right)\right) \\
&= \tfrac{1}{4}\sum_{i\neq j} \vec{r}_{ij} \left(\sum_{k\subset i, l\subset j} \vec{f}_{kl,\text{inter}}\left(\vec{v}_{a,k} + \vec{v}_{a,l}\right)\right) \\
&= \tfrac{1}{2}\sum_{i>j} \vec{r}_{ij} \left(\sum_{k\subset i, l\subset j} \vec{f}_{kl,\text{inter}}\left(\vec{v}_{a,k} + \vec{v}_{a,l}\right)\right).
\end{aligned} \tag{A4}$$

Substituting Eq. (A3) into Eq. (A1), we obtain

$$\vec{q} = \frac{1}{V}\left(\sum_i \vec{v}_i E_i + \tfrac{1}{2}\sum_{i>j} \vec{r}_{ij} \left(\sum_{k\subset i, l\subset j} \vec{f}_{kl,\text{inter}} \cdot \left(\vec{v}_{a,k} + \vec{v}_{a,l}\right)\right)\right). \tag{A5}$$

REFERENCES

[1] S. S. Sazhin, "Advanced models of fuel droplet heating and evaporation," Prog. Energy Combust. Sci. **32**, 162 (2006).
[2] S. S. Sazhin, I. N. Shishkova, A. P. Kryukov, V. Y. Levashov, and M. R. Heikal, "Evaporation of droplets into a background gas: Kinetic modelling," Int. J. Heat Mass Transfer **50**, 2675 (2007).
[3] B.-Y. Cao, J.-F. Xie, and S. S. Sazhin, "Molecular dynamics study on evaporation and condensation of *n*-dodecane at liquid-vapor phase equilibria," J. Chem. Phys. **134**, 164309 (2011).
[4] J.-F. Xie, S. S. Sazhin, and B.-Y. Cao, "Molecular dynamics study of the processes in the vicinity of the n-dodecane vapour/liquid interface," Phys. Fluids **23**, 112104 (2011).
[5] G. Nagayama, M. Takematsu, and T. Tsuruta, "Condensation/evaporation coefficient of chain molecules," Trans. Jpn. Soc. Mech. Eng. **79**, 2149 (2013).
[6] G. Nagayama, M. Takematsu, H. Mizuguchi, and T. Tsuruta, "Molecular dynamics study on condensation/evaporation coefficients of chain molecules at liquid–vapor interface," J. Chem. Phys. **143**, 014706 (2015).
[7] R. Tao, K. Huang, H. Tang, and D. Bell, "Electrorheology leads to efficient combustion," Energy Fuels **22**, 3785 (2008).
[8] A. H. Persad and C. A. Ward, "Expressions for the evaporation and condensation in the Hertz-Knudsen relation," Chem. Rev. **116**, 7727 (2016).
[9] H. Hertz, "Ueber die Verdunstung der Flüssigkeiten, insbesondere des Quecksilbers, im luftleeren Raume," Ann. Phys. **253**, 177 (1882).
[10] M. Knudsen, *Kinetic Theory of Gases*, 3rd ed. (London Methuene, London, 1950).
[11] R. W. Schrage, *A Theoretical Study of Interphase Mass Transfer* (Columbia University Press, New York, 1953).
[12] F. O. Goodman and H. Y. Wachman, *Dynamics of Gas-Surface Scattering* (Academic Press, New York, 1976), pp. 23–31.
[13] V. P. Carey, *Liquid–Vapor Phase-Change Phenomena* (Hemisphere, Publishing House, New York, 1992).
[14] R. Holyst and M. Litniewski, "Heat transfer at the nanoscale: Evaporation of nanodroplets," Phys. Rev. Lett. **100**, 055701 (2008).
[15] J. Gonzalez, J. Ortega, and Z. Liang, "Prediction of thermal conductance at liquid-gas interfaces using molecular dynamics simulations," Int. J. Heat Mass Transfer **126**, 1183 (2018).
[16] Agency for Toxic Substances and Disease Registry (ATSDR), *Toxicological Profile for Fuel Oils* (U.S. Department of Health and Human Services, Public Health Service, Atlanta, GA, 1995).
[17] Z. Liang, T. Biben, and P. Keblinski, "Molecular simulation of steady-state evaporation and condensation: Validity of the Schrage relationships," Int. J. Heat Mass Transfer **114**, 105 (2017).
[18] Z. Liang and P. Keblinski, "Molecular simulation of steady-state evaporation and condensation in the presence of a non-condensable gas," J. Chem. Phys. **148**, 064708 (2018).
[19] Z. Liang, W. Evans, T. Desai, and P. Keblinski, "Improvement of heat transfer efficiency at solid-gas interfaces by self-assembled monolayers," Appl. Phys. Lett. **102**, 061907 (2013).
[20] Z. Liang, W. Evans, and P. Keblinski, "Equilibrium and nonequilibrium molecular dynamics simulations of thermal conductance at solid-gas interfaces," Phys. Rev. E **87**, 022119 (2013).
[21] Z. Liang and P. Keblinski, "Parametric studies of the thermal and momentum accommodation of monoatomic and diatomic gases on solid surfaces," Int. J. Heat Mass Transfer **78**, 161 (2014).

[22]S. K. Nath, F. A. Escobedo, and J. J. de Pablo, "On the simulation of vapor–liquid equilibria for alkanes," J. Chem. Phys. **108**, 9905 (1998).
[23]R. Khare, J. de Pablo, and A. Yethiraj, "Rheological, thermodynamic, and structural studies of linear and branched alkanes under shear," J. Chem. Phys. **107**, 6956 (1997).
[24]S. H. Pine, *Organic Chemistry*, 2nd ed. (McGraw-Hill, New York, 1964).
[25]P. Padilla and S. Toxvaerd, "Self-diffusion in *n*-alkane fluid models," J. Chem. Phys. **94**, 5650 (1991).
[26]W. L. Jorgensen, J. D. Madura, and C. J. Swenson, "Optimized intermolecular potential functions for liquid hydrocarbons," J. Am. Chem. Soc. **106**, 6638 (1984).
[27]B. Smit, S. Karaborni, and J. I. Siepmann, "Computer simulations of vapour liquid phase equilibria of n-alkanes," J. Chem. Phys. **102**, 2126 (1995).
[28]D. Frenkel and B. Smit, *Understanding Molecular Simulation* (Springer, Berlin, 2002).
[29]S. M. Foiles, M. I. Baskes, and M. S. Daw, "Embedded-atom-method functions for the fcc metals Cu, Ag, Au, Ni, Pd, Pt, and their alloys," Phys. Rev. B **33**, 7983 (1986).
[30]A. K. Rappe, C. J. Casewit, K. S. Colwell, W. A. Goddard, and W. M. Skiff, "UFF, a full periodic table force field for molecular mechanics and molecular dynamics simulations," J. Am. Chem. Soc. **114**, 10024 (1992).
[31]H. J. C. Berendsen, J. P. M. Postma, W. F. Van Gunsteren, A. DiNola, and J. R. Haak, "Molecular dynamics with coupling to an external bath," J. Chem. Phys. **81**, 3684 (1984).
[32]E. W. Lemmon, M. O. McLinden, and D. G. Friend, "Thermophysical properties of fluid systems," in *NIST Chemistry WebBook*, NIST Standard Reference Database Number 69 (NIST, 2018).
[33]P. J. Linstrom and W. G. Mallard, National Institute of Standards and Technology, Gaithersburg, MD (retrieved September 12, 2019).
[34]T. Tsuruta and G. Nagayama, "Molecular dynamics studies on the condensation coefficient of water," J. Phys. Chem. B **108**, 1736 (2004).
[35]K. Wark, *Generalized Thermodynamic Relationships. Thermodynamics*, 5th ed. (McGraw-Hill, New York, 1988), p. 509.
[36]S. W. I. Siu, K. Pluhackova, and R. A. Böckmann, "Optimization of the OPLS-AA force field for long hydrocarbons," J. Chem. Theory Comput. **8**, 1459 (2012).
[37]P. W. Atkins and J. de Paula, *Physical Chemistry*, 8th ed., edited by W. H. Freeman (Oxford, New York, 2006), pp. 291–453.
[38]Z. Liang and H.-L. Tsai, "Calculation of thermophysical properties of CO_2 gas using an *ab initio* potential model," Mol. Phys. **108**, 1285 (2010).
[39]M. P. Allen and D. J. Tildesley, *Computer Simulation of Liquids* (Clarendon Press, Oxford, 2000).
[40]S. Chandrasekhar, Rev. Mod. Phys. **15**, 1–89 (1943).
[41]T. Ishiyama, T. Yano, and S. Fujikawa, "Molecular dynamics study of kinetic boundary condition at an interface between argon vapor and its condensed phase," Phys. Fluids **16**, 2899 (2004).
[42]P. Jund and R. Jullien, "Molecular-dynamics calculation of the thermal conductivity of vitreous silica," Phys. Rev. B **59**, 13707 (1999).